Magnetic-field analysis of an MHD channel in a liquid-metal circulation system of a prototype GenIV sodium fast reactor

Authors: Lee, G., & Kim, H.R*.

Journal Information:

- **Journal:** Annals of Nuclear Energy
- **Year:** 2018
- **Volume:** 115
- **Pages:** 343-351
- **DOI:** https://doi.org/10.1016/j.anucene.2018.01.049

Magnetic-field analysis of an MHD channel in a liquid-metal circulation system of a prototype GenIV sodium fast reactor

Geun Hyeong Lee, Hee Reyoung Kim*

Ulsan National Institute of Science and Technology, Department of Nuclear Engineering, Ulsan 689-798, Republic of Korea

Abstract

A helical-type direct current (DC) electromagnetic pump with a developed pressure of 10 kPa and flow rate of 0.005 m^3/s was analyzed at a temperature of 226 °C for an active decay heat-removal system (ADHRS) of a prototype GenIV sodium fast reactor. The rectangular-type DC electromagnetic pump, which was selected for the ADHRS, requires a very large current (>1000 A). The helical-type DC electromagnetic pump was considered to provide multiple current to a pump duct to reduce the input current requirement. The magnetic flux density of a permanent magnet is one of the important factors that determine the performance of the electromagnetic pump. The magnetic field for the flow channel of the helical-type DC electromagnetic pump was analyzed in which a Sm_2Co_{17} permanent magnet was used to generate the Lorentz force for the circulation of liquid metal. The Lorentz force, which directly affected the developed pressure of the electromagnetic pump, was increased proportional to the magnetic flux density, which led to the increase in the velocity of the liquid metal in the flow channel. The permanent magnet in the +z and −z directions and the ferromagnetic material added in the r direction increased the magnitude of the magnetic flux density, which led the magnetic flux line to the flow channel. The arrangement of the permanent magnet system showed the optimized geometry of the inner ferromagnetic material with a radius of 110 mm and outer ferromagnetic material with a thickness of 30 mm and height of 70 mm. The average value of the magnetic flux density in the liquid-metal flow channel was 0.848 T under maximum condition by considering the mechanical and spatial restrictions.

Keywords: magnetic flux density, helical-type DC electromagnetic pump, permanent magnet, ferromagnetic material

Nomenclature

B	Magnetic flux density [T]
B_e	Magnetic flux density of the permanent magnet [T]

B_i	Magnetic flux density of the electrode stub [T]
B_t	Total magnetic flux density [T]
E	Electric field [kg·m/(s^3·A)]
E_t	Total electric field [kg·m/(s^3·A)]
f	Force density [kg/(s^2·m^2)]
H	Magnetic-field intensity [A/m]
H_m	Magnetic-field intensity of the permanent magnet [A/m]
J	Current density [A/m^2]
J_t	Total current density [A/m^2]
M	Magnetization [A/m]
t	Time [s]
v	Velocity of fluid [m/s]
ε_0	Permittivity in vacuum [F/m]
μ_0	Permeability in vacuum [H/m]
μ_r	Relative permeability
σ	Electrical conductivity of liquid metal [1/(Ω · m)]
χ_m	Magnetic susceptibility

1. Introduction

Electromagnetic pumps are used to circulate liquid metal, instead of mechanical pumps, owing to their advantages such as no moving and sealing parts while eliminating the possibility of liquid-metal leak (Kim, 2014). A direct current (DC) electromagnetic pump was considered for an active decay heat-removal system (ADHRS) to transport liquid sodium to a prototype GenIV sodium fast reactor (PGSFR) (Kim, 2014). The ADHRS considers the electromagnetic pump driven by an electromagnetic force generated from the Lorentz force for the forced sodium circulation in the sodium loop, which contains a blower with finned-tube sodium-to-air heat exchanger (FDHX), as shown in Fig. 1 (Lee, 2013). The helical-type DC electromagnetic pump is adopted to circulate liquid sodium with high electrical conductivity (Ohse, 1985; Baker, 1987) via an electromagnetic force (or Lorentz force) generated from the vector product of the current density and magnetic field (Nashine, 2007; Gutierrez, 1965). This process is adopted because the electromagnetic pump structure has

no sealing part and an impeller, which can cause failure during the transportation of high-reactivity liquid sodium. In particular, the helical-type DC electromagnetic pump requires a low current compared with a rectangular-type one because it can obtain multiple current from the geometry of the pump duct. Magnetic flux density is one of the main factors that contribute to the generation of the pumping force from the Lorentz force and the induced electromotive force in the circular channel of the helical-type DC electromagnetic pump, which affects the specification of the flow rate and the developed pressure of the electromagnetic pump (Nashine, 2006; Blake, 1957). The magnetic flux density generated from the combined arrangement of the permanent magnet and ferromagnetic material in the flow channel in the electromagnetic pump is analyzed, where the Lorentz force produced by the vector product of the externally driven current and magnetic field in the liquid-metal flow inside the channel drives the pump (Oka, 2012). The pumping force appears as a function of the magnetic flux density and pump geometrical variables where a higher magnetic flux density is needed to enhance the hydraulic efficiency of the helical-type DC electromagnetic pump (Kikuchi, 1977). In the present study, the magnetic field is analyzed and optimized in terms of the arrangement of the permanent magnet according to the direction of the magnetic field and the geometrical size of the ferromagnetic material.

2. Analysis of helical-type DC electromagnetic pump

The helical-type DC electromagnetic pump (Marti, 2015; Lee, 2017) contains four types of components: ferromagnetic material, permanent magnet (Zhu, 1992), electrode stub, and pump duct (Ho, 1977), as shown by the schematic in Fig. 2. The Lorentz force is generated by the vector product of the current of the electrode stub and the magnetic flux density of the permanent magnet where the liquid metal flows in the θ direction that receives the electromagnetic force generated by the current in the z direction and the magnetic flux density in the r direction, as shown in Fig. 2 (Bennecib, 2009). The magnetic flux density is determined by Maxwell's equation of Ampere's law, Faraday's law, and Gauss's law for magnetism and Ohm's law expressed in Eqs. (1)–(4) using the finite element method (FEM) (Moffatt, 1978; Arumugam, 1985; Hughes, 1995).

$$\text{Ampere's law: } \nabla \times \vec{B} = \mu_0 (\vec{J} + \varepsilon_0 \frac{\partial E}{\partial t}) \tag{1}$$

$$\text{Faraday's law: } \nabla \times \vec{E} = -\frac{\partial \vec{B}}{\partial t} \tag{2}$$

$$\text{Gauss's law for magnetism: } \nabla \cdot \vec{B} = 0 \tag{3}$$

$$\text{Ohm's law: } \vec{J} = \sigma(\vec{E} + \vec{v} \times \vec{B}) \tag{4}$$

The equations of the electric field, current density, magnetic flux density, and velocity of the fluid are expressed in Eqs. (5)–(10). The electric field in the θ direction is eliminated due to the symmetry of the pump duct. The magnetic flux density is divided into the external magnetic flux density of the permanent magnet and the induced magnetic flux density of the electrode stub. The external magnetic flux density in the θ direction is eliminated due to the symmetry of the permanent magnet and ferromagnetic material. The velocity of the fluid has only a θ-direction component because the pump duct is built in the θ direction. The z-direction component is negligible because the pump-duct circumference is much higher than the pump-duct radius. In other words, the angle of the pump duct is almost equal to zero.

$$\vec{E}_t(r,\theta,z) = E_r\hat{r} + E_z\hat{z} \tag{5}$$

$$\vec{J}_t(r,\theta,z) = J_r\hat{r} + J_\theta\hat{\theta} + J_z\hat{z} \tag{6}$$

$$\vec{B}_t(r,\theta,z) = \vec{B}_i(r,\theta,z) + \vec{B}_e(r,\theta,z) \tag{7}$$

$$\vec{B}_i(r,\theta,z) = B_{i,r}\hat{r} + B_{i,\theta}\hat{\theta} + B_{i,z}\hat{z} \tag{8}$$

$$\vec{B}_e(r,\theta,z) = B_{e,r}\hat{r} + B_{e,z}\hat{z} \tag{9}$$

$$\vec{v}(r,\theta,z) = v_\theta\hat{\theta} \tag{10}$$

Ampere's law in Eq. (1) is expressed in Eqs. (11)–(14) using the curl operator calculation in a cylindrical coordinate. The $\frac{\partial}{\partial\theta}$ term of the magnetic flux density is eliminated due to the symmetry of the permanent magnet, ferromagnetic material, and current density in the flow channel of the helical-type DC electromagnetic pump. The external magnetic flux density is created by some rotating electrons in which the circulating current is microscopically small. Therefore, only the induced magnetic flux density is considered to calculate Ampere's law. The electric field due to the direct current remains constant as time changes. Thus, the rate of change in the electric field term disappears. The magnetic permeability is expressed as

$$\nabla \times \vec{B}_i = \mu_0\vec{J}_t \tag{11}$$

$$\nabla \times \vec{B}_i = \frac{\partial B_{i,\theta}}{\partial z}\hat{r} + \left(\frac{\partial B_{i,r}}{\partial z} - \frac{\partial B_{i,z}}{\partial r}\right)\hat{\theta} + \frac{1}{r}\frac{\partial (rB_{i,\theta})}{\partial r}\hat{z} \tag{12}$$

$$\mu_0 \vec{J_t} = \mu_0 (J_r \hat{r} + J_\theta \hat{\theta} + J_z \hat{z}) \tag{13}$$

$$\frac{\partial B_{i,\theta}}{\partial z} = \mu_0 J_r, \frac{\partial B_{i,r}}{\partial z} - \frac{\partial B_{i,z}}{\partial r} = \mu_0 J_\theta, \frac{1}{r}\frac{\partial (rB_{i,\theta})}{\partial r} = \mu_0 J_z. \tag{14}$$

In the same manner, Faraday's law in Eq. (2) is expressed by Eqs. (15)–(17). The magnetic flux density is not a time-varying function because the helical-type DC electromagnetic pump employs permanent magnet and DC. The $\frac{\partial}{\partial \theta}$ component of the electric field is also deleted due to the symmetry of the permanent magnet, ferromagnetic material, and current density in the flow channel.

$$\nabla \times \vec{E}_t = 0 \tag{15}$$

$$\nabla \times \vec{E}_t = \left(\frac{\partial E_r}{\partial z} - \frac{\partial E_z}{\partial r}\right)\hat{\theta} \tag{16}$$

$$\frac{\partial E_z}{\partial r} - \frac{\partial E_r}{\partial z} = 0 \tag{17}$$

Gauss's law for magnetism in Eq. (3) is expressed using a divergence operator in the cylindrical coordinate, as expressed in Eqs. (18)–(22). The divergence in the total magnetic flux density is zero, and the divergence in the external magnetic flux density of permanent magnet is zero. Therefore, the induced magnetic flux density is zero. The $\frac{\partial}{\partial \theta}$ component of the electric field is also deleted due to the symmetry of the helical-type DC electromagnetic pump.

$$\nabla \cdot \vec{B}_t = \nabla \cdot \vec{B}_i + \nabla \cdot \vec{B}_e = 0 \tag{18}$$

$$\nabla \cdot \vec{B}_e = 0 \tag{19}$$

$$\nabla \cdot \vec{B}_i = 0 \tag{20}$$

$$\nabla \cdot \vec{B}_e = \frac{1}{r}\frac{\partial (rB_{e,r})}{\partial r} + \frac{\partial B_{e,z}}{\partial z} = 0 \tag{21}$$

$$\nabla \cdot \vec{B}_i = \frac{1}{r}\frac{\partial (rB_{i,r})}{\partial r} + \frac{\partial B_{i,z}}{\partial z} = 0 \tag{22}$$

Ohm's law in Eq. (4) is expressed using the vector product, as presented in Eqs. (23)–(26). The current

density in the θ direction is zero because the electric field -and the vector product of the velocity and magnetic flux density in the θ direction are zero.

$$\vec{J}_t = \sigma(\vec{E}_t + \vec{v} \times \vec{B}_t) \tag{23}$$

$$\vec{J}_t = J_r\hat{r} + J_\theta\hat{\theta} + J_z\hat{z} \tag{24}$$

$$\sigma(\vec{E}_t + \vec{v} \times \vec{B}_t) = \sigma\{(E_r + v_\theta B_{i,z} + v_\theta B_{e,z})\hat{r} + (E_z - v_\theta B_{i,r} - v_\theta B_{e,r})\hat{z}\} \tag{25}$$

$$J_r = \sigma(E_r + v_\theta B_{i,z} + v_\theta B_{e,z}), J_\theta = 0, J_z = \sigma(E_z - v_\theta B_{i,r} - v_\theta B_{e,r}) \tag{26}$$

Therefore, the relationship between the electric field and magnetic flux density is obtained by combining Eqs. (14) and (26), as expressed in Eqs. (27) and (28).

$$\frac{\partial B_{i,r}}{\partial z} = \frac{\partial B_{i,z}}{\partial r} \tag{27}$$

$$\frac{1}{\mu_0\sigma}\frac{\partial B_{i,\theta}}{\partial z} = E_r + v_\theta B_{i,z} + v_\theta B_{e,z}, \frac{1}{\mu_0\sigma}\frac{1}{r}\frac{\partial(rB_{i,\theta})}{\partial r} = E_z - v_\theta B_{i,r} - v_\theta B_{e,r} \tag{28}$$

The electric field is deleted using Eq. (17). Therefore, the relationship of the magnetic flux density is given in Eq. (29).

$$\frac{1}{\mu_0\sigma}\left\{\frac{\partial^2 B_{i,\theta}}{\partial z^2} - \frac{1}{r}\frac{\partial^2(rB_{i,\theta})}{\partial r^2} + \frac{1}{r^2}\frac{\partial\left(rB_{i,\theta}\right)}{dr}\right\} = v_\theta(B_{i,z} + v_\theta B_{e,z} + v_\theta B_{i,r} + v_\theta B_{e,r}) \tag{29}$$

The magnetic flux density of the flow channel is analyzed by applying the permanent magnet (Sm_2Co_{17}) magnetic coercivity and the ferromagnetic material (1010 steel) magnetic permeability using FEM. The magnetization can be expressed by Eq. (30) by considering the permanent magnet and ferromagnetic material.

$$\vec{M} = \chi_m\vec{H} + \vec{H}_m \tag{30}$$

The total magnetic flux density in the helical-type DC electromagnetic pump, as expressed in Eq. (31), is calculated by considering the permanent magnetic field (H_m) and independent local magnetic field.

$$\vec{B} = \mu_0(\vec{H} + \vec{M}) = \mu_0\mu_r\vec{H} + \mu_0\vec{H}_m \tag{31}$$

The boundary conditions of the magnetic flux density and magnetic-field intensity are applied between the different magnetic permeability materials using Eqs. (32) and (33).

$$\vec{H}_{t,1} = \vec{H}_{t,2} \tag{32}$$

$$\vec{B}_{n,1} = \vec{B}_{n,2} \tag{33}$$

The tangential component of the magnetic-field intensity and normal component of the magnetic flux density between high (ferromagnetic material) and low (air, stainless steel 316L, C103, and Sm_2Co_{17}) magnetic permeability materials at the interface are applied to determine the magnetic flux density and flux line of the helical-type DC electromagnetic pump using the ANSYS Maxwell code simulation.

The helical-type DC electromagnetic pump requires a Lorentz force to create the velocity of the fluid in the narrow channel, as shown in Eq. (34). The θ-direction Lorentz force only affects the velocity of the fluid, as expressed in Eq. (10) and presented in Eq. (35).

$$\vec{f} = \vec{J} \times \vec{B} \tag{34}$$

$$f_\theta = J_z B_r - J_r B_z \tag{35}$$

The vector product of the current density in the z direction and the magnetic flux density in the r direction can be neglected compared with the vector product of the current density in the r direction and the magnetic flux density in the z direction, as expressed by Eqs. (26) and (35). The electric field in the r direction can be neglected compared with that in the z direction because current flows along the z direction and the gap in the pump duct is narrow. The induced magnetic flux density in the r and z directions can be ignored because the electric field in the r direction is negligible. The external magnetic flux density in the z direction in the flow channel is negligible compared with that in the r direction because the ferromagnetic material induces magnetic flux along the r direction. The magnetic flux density in the r direction is dominantly influenced by the Lorentz force. Therefore, the magnetic flux density in the r direction is analyzed using the ANSYS Maxwell code simulation. The region of the flow channel is determined to consider the external heat system at the pump-duct region, which requires at least 6 mm in the length direction, including the insulator. The diameter of the pump duct is 10 mm considering the space and pump weight. Therefore, the pump-duct length is determined to be 16 mm, which is equal to the diameter of the pump duct plus the external heat system, and the height is 200 mm, which represents 20 turns of the pump duct.

3. Results and discussion

The magnetic flux density in the r direction was analyzed at a flow channel region with a length of 16 mm and height of 200 mm, which was located in the duct of the electromagnetic pump, as shown in Fig. 2. The Sm_2Co_{17} permanent magnet with a high maximum working temperature of 300 ℃ and the 1010 steel ferromagnetic material with a high magnetic permeability of more than 2000 were adopted to generate a magnetic field and to induce a magnetic flux, respectively. The permanent magnet magnetized in the +z and −z directions was added to increase the magnetic flux density in the helical-type DC electromagnetic pump. The considered pump-duct material was stainless steel 316L to prevent a chemical reaction between the liquid metal and pump duct and distortion in the magnetic field that passes through the flow channel. The analysis region of the magnetic flux density is shown in Fig. 3. The magnetic flux density of a ring-type permanent magnet with magnetization in the radial direction is shown in Fig. 4. This figure shows that the end part of the permanent magnet had the highest magnetic flux density due to its end effect where the flux line at end part and the magnetic flux density were reduced because they were very far from the permanent magnet as the magnetic flux line was concentrated at the end part of the permanent magnet. The density of the flux line was reduced as it became very far from the permanent magnet due to the flux line, as shown in Fig. 5. The flux line sparsely existed and had many z-direction components compared with the r-direction components because no magnetic flux inducement materials were present. The 1010 steel ferromagnetic material with a high relative magnetic permeability (~4000) was used to increase the magnetic flux density and to provide more r-direction component magnetic fluxes. The magnitude and tendency of the magnetic flux density assumed the geometrical structure of the ferromagnetic material, and airspace existed at the outer surface, as shown in Fig. 6. We verified this result from the comparison with Xia's analysis, which represented the magnetic flux density in the same cylindrical geometry as a magnetic machine (Xia, 2004). According to the analysis, the peak magnetic flux density was approximately 0.85 T, and the peak shown in Fig. 6 was 0.93 T. The magnetic flux density increased and was equalized at the middle part of the analysis region due to the increase in the magnetization. The flux line was concentrated in the analysis region, and it almost lay in the r direction in the middle part to increase the magnetic flux density and equality due to the magnetization, as shown in Fig. 7. A permanent magnet magnetized along the +z and −z directions was added to the helical-type DC electromagnetic pump to provide r-direction magnetic flux at the end part (Babic, 2008; Xiao-Fan, 2004). Fig. 8 shows the magnetic flux density distribution in the analysis region with the permanent magnet magnetized along the z direction. The permanent

magnet reinforced the magnetic flux density at the end part because more flux lines were created by the permanent magnet magnetized along the z direction, as shown in Fig. 9. Fig. 10 shows the comparison of the magnetic flux density due to the existence of permanent magnets with z-direction magnetization at the middle point of the pump-duct region length. The mean value of the magnetic flux density increased by 8.8% from 0.786 to 0.855 T due to the z-direction magnetization, and it was further equalized at the middle part due to the increase in the end-part flux line. The equalized magnetic flux density reduced the electromotive-force effect on the helical-type DC electromagnetic pump, which is one of the main reasons of the pressure loss, and provided equalized force in the flow channel. The size of the ferromagnetic material was optimized to enhance the magnetic flux density by minimizing the unnecessary weight. The magnetic flux density increased as the distance of the permanent magnets decreased because the flux line decreased farther from the permanent magnets. Meanwhile, the magnetic flux density decreased as the thickness of the ferromagnetic material decreased because the magnetization increased. Therefore, the thickness of the inner ferromagnetic material had an optimum point of 110 mm, as shown in Fig. 11, to satisfy 0.915 T of maximum magnetic flux density. The shape and magnitude of the magnetic flux density line at the middle point along the pump-duct region length varied as the thickness and height of the outer ferromagnetic material varied. The shape changed to linear at the middle point due to the increased flux lines at the middle part, and the magnitude of the magnetic flux density had a maximum point of 0.915 T as the thickness and height of the outer ferromagnetic material increased, as shown in Figs. 12 and 13. The thickness and height of the outer ferromagnetic material attained a saturation point because the flux line had a limit at a thickness of 30 mm and height of 460 mm, which reduced the total weight of the helical-type DC electromagnetic pump.

4. Conclusion

The magnetic field of the flow channel in a helical-type DC electromagnetic pump was analyzed to maximize the magnetic flux density and enhance the pump efficiency using FEM through ANSYS Maxwell code simulation. The additional arrangement of the permanent magnet along the +z and −z directions contributed to the increase and homogeneity in the magnetic flux density in the helical-type DC electromagnetic pump. The ferromagnetic material was considered to increase the r-direction magnetic flux density at the flow channel of the helical-type DC electromagnetic pump. The thickness and height of the inner and outer ferromagnetic materials were optimized so that the inner material had a radius of 100 mm and the outer material was 30-mm thick and 460-mm long to maximize the magnetic flux density to an average value of 0.855 T.

References

Babic, S. I., Akyel, C., 2008, Improvement in the analytical calculation of the magnetic field produced by permanent magnet rings. Progress in Electromagnetics Research C, 5, 71-82.

Baker, R.S., Tessier, M.J., 1987, Handbook of electromagnetic pump technology, Elsevier, New York.

Ho, C.Y., Chu, T.K., 1977, Electrical resistivity and thermal conductivity of nine selected AISI stainless steels, CINDAS Report 45, Washington.

Lee, G. H., Kim, H. R., 2017, NUMERICAL INVESTIGATION AND COMPARISON OF THE RECTANGULAR, CYLINDRICAL, AND HELICAL-TYPE DC ELECTROMAGNETIC PUMPS, Magnetohydrodynamics, 53(2), 429-438.

Lee, H. Y., Eoh, J. H., Lee, Y. B., 2013, High temperature design of finned-tube sodium-to-air heat exchanger in a sodium test loop, Nuclear Engineering and Design, 265, 833-840.

Marti, F., Guetschow, P., Momozaki, Y., Nolen, J. A., 2015, Development of a liquid lithium charge stripper for FRIB, Proceedings of HIAT2015, Japan.

Nashine, B.K., Dash, S.K., Gurumurthy, K., Kale, U., Sharma, V.D., Prabhaker, R., Rajan, M., Vaidyanathan, G., 2007, Performance testing of indigenously developed DC conduction pump for sodium cooled fast reactor, Indian Journal of Engineering & Material Science, 14, 209-214.

Ohse, R.W., 1985, Handbook of thermodynamic and transport properties of alkali metals, 1985, Oxford.

Oka, T., Kawasaki, N., Fukui S., Ogawa, J., Sato, T., Terasawa, T., Itoh, Y., Yabuno, R., 2012, Magnetic field distribution of permanent magnet magnetized by static magnetic field generated by HTS bulk magnet, IEEE Transaction on Applied Superconductivity, 22(3), 9502304-9502304.

Xia, Z. P., Zhu, Z. Q., Howe, D., 2004. Analytical magnetic field analysis of Halbach magnetized permanent-magnet machines. IEEE Transactions on Magnetics, 40(4), 1864-1872.

Xiao-Fan, G., Yong, Y., Xiao-Jing, Z., 2004, Analytic expression of magnetic field distribution of rectangular permanent magnets. Applied Mathematics and Mechanics, 25(3), 297-306.

Zhu, Z. Q., Howe, D., 1992, Analytical prediction of the cogging torque in radial-field permanent magnet brushless motors. IEEE Transactions on Magnetics, 28(2), 1371-1374.

Moffatt, H. K., 1978, Field generation in electrically conducting fluids, Cambridge University Press, New York.

Kikuchi, S., Murakami, K., 1977, Behavior of a new DC electromagnetic pump using superconducting magnet, IEEE Transactions on Magnetics, 13(5), 1559-1561.

Nashine, B. K., Dash, S. K., Gurumurthy, K., Rajan, M., Vaidyanathan, G., 2006, Design and testing of DC conduction pump for sodium cooled fast reactor, In 14th International Conference on Nuclear Engineering, American Society of Mechanical Engineers.

Gutierrez, A. U., Heckathorn, C. E., 1965, Electromagnetic pumps for liquid metals, Naval Postgraduate School, California.

Blake, L. R., 1957, Conduction and induction pumps for liquid metals, Proceedings of the IEE-Part A: Power Engineering, 104(13), 49-67.

Arumugam, R., Lowther, D., Krishnan, R., Lindsay, J., 1985, Magnetic field analysis of a switched reluctance motor using a two dimensional finite element model, IEEE Transactions on Magnetics, 21(5), 1883-1885.

Bennecib, N., Drid, S., Abdessemed, R., 2009, Numerical investigation of flow in a new DC pump MHD, Journal of Applied Fluid Mechanics, 2(2), 23-28.

Kim, D., Hong, J., Lee, T., 2014, Design of DC conduction pump for PGSFR active decay heat removal system, Transactions of the Korean Nuclear Society Spring Meeting, Korea.

Kim, H. R., 2014, The design and fabrication of a small MHD pump for liquid sodium circulation, Annals of Nuclear Energy, 73, 162-167.

Hughes, M., Pericleous, K. A., Cross, M., 1995, The numerical modelling of DC electromagnetic pump and brake flow. Applied Mathematical Modelling, 19(12), 713-723.

Figure captions

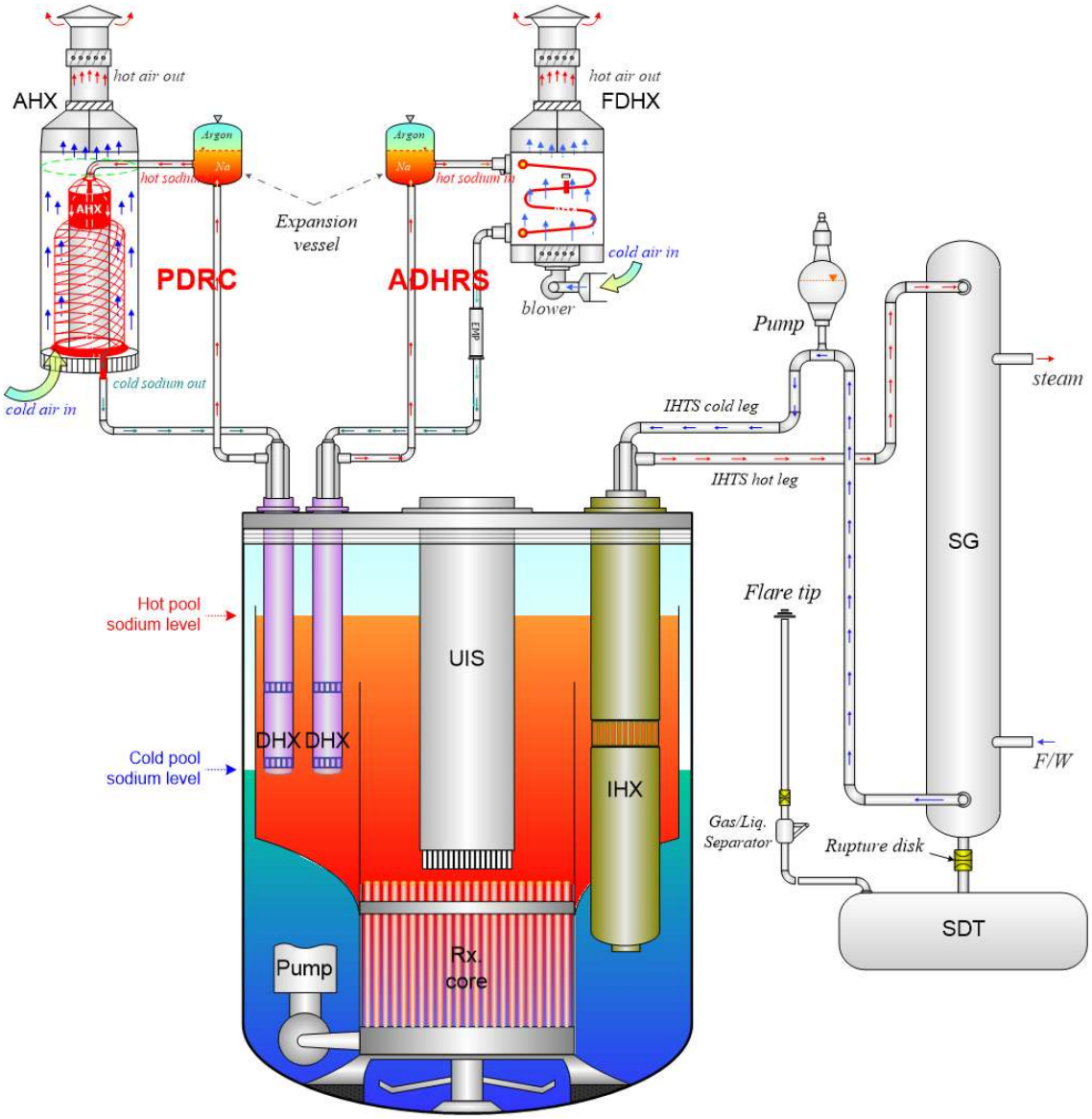
AHX
hot air out
Argon
Na
hot sodium
AHX
cold air in
cold sodium out
PDRC
Expansion vessel
Argon
Na
hot sodium in
ADHRS
hot air out
FDHX
cold air in
blower
EMP
Pump
steam
IHTS cold leg
IHTS hot leg
SG
Flare tip
Hot pool sodium level
Cold pool sodium level
UIS
DHX DHX
IHX
Gas/Liq. Separator
Rupture disk
F/W
SDT
Pump
Rx. core

Fig. 1

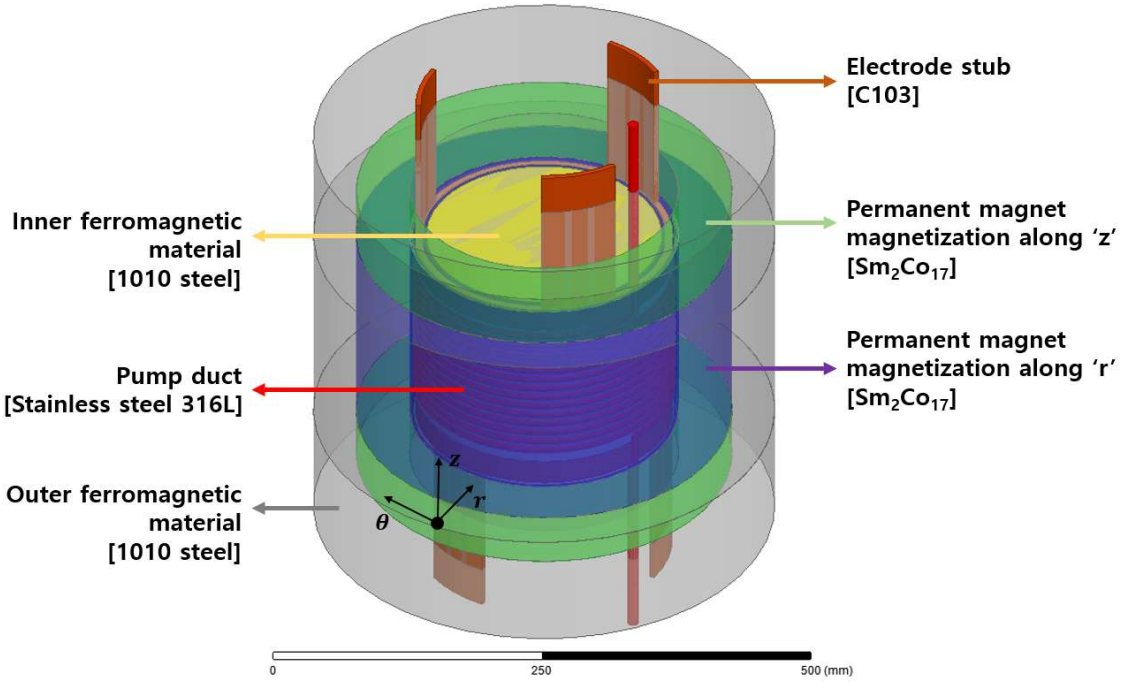
Electrode stub
[C103]
Inner ferromagnetic
material
[1010 steel]
Permanent magnet
magnetization along 'z'
[Sm_2Co_{17}]
Permanent magnet
magnetization along 'r'
[Sm_2Co_{17}]
Pump duct
[Stainless steel 316L]
Outer ferromagnetic
material
[1010 steel]
z
r
θ
0
250
500 (mm)

Fig. 2

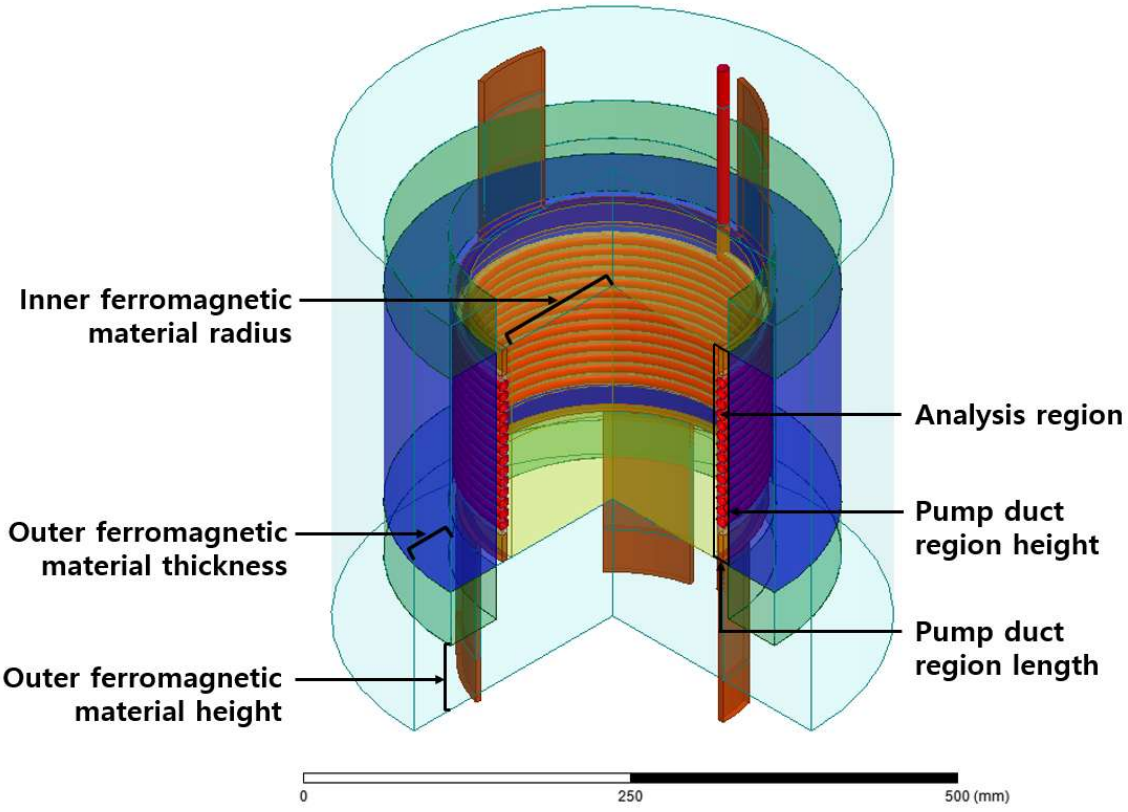
Inner ferromagnetic
material radius
Analysis region
Outer ferromagnetic
material thickness
Pump duct
region height
Pump duct
region length
Outer ferromagnetic
material height
0
250
500 (mm)

Fig. 3

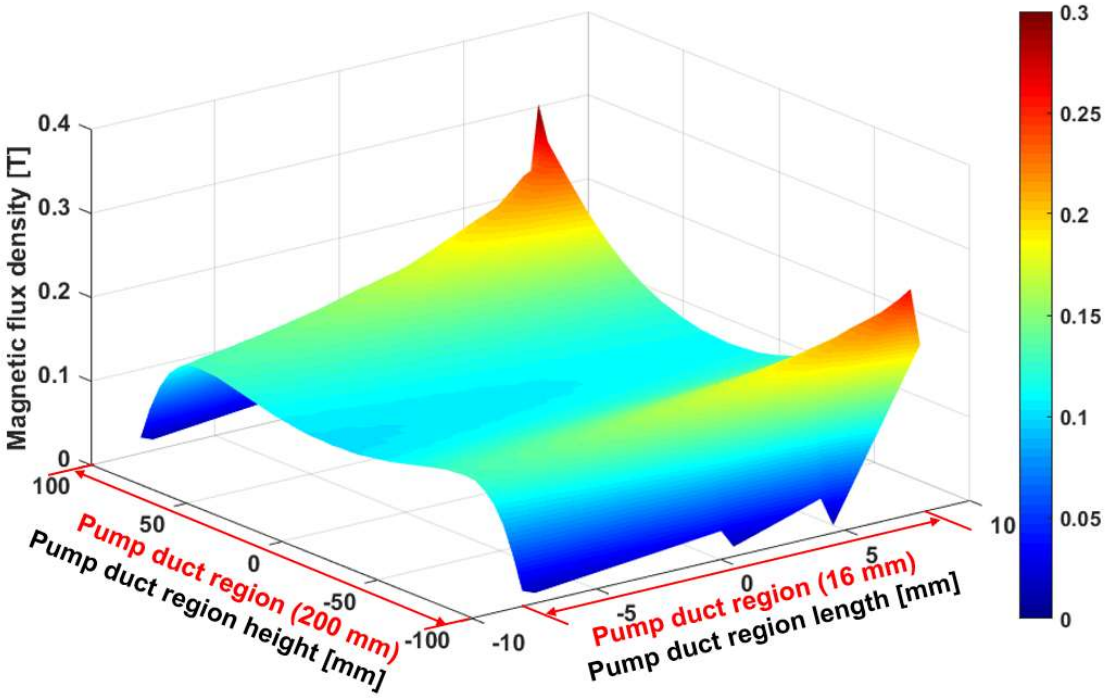
Magnetic flux density [T]
0.4
0.3
0.2
0.1
0
100
50
0
-50
-100
Pump duct region (200 mm)
Pump duct region height [mm]
-10
-5
0
5
10
Pump duct region (16 mm)
Pump duct region length [mm]
0.3
0.25
0.2
0.15
0.1
0.05
0

Fig. 4

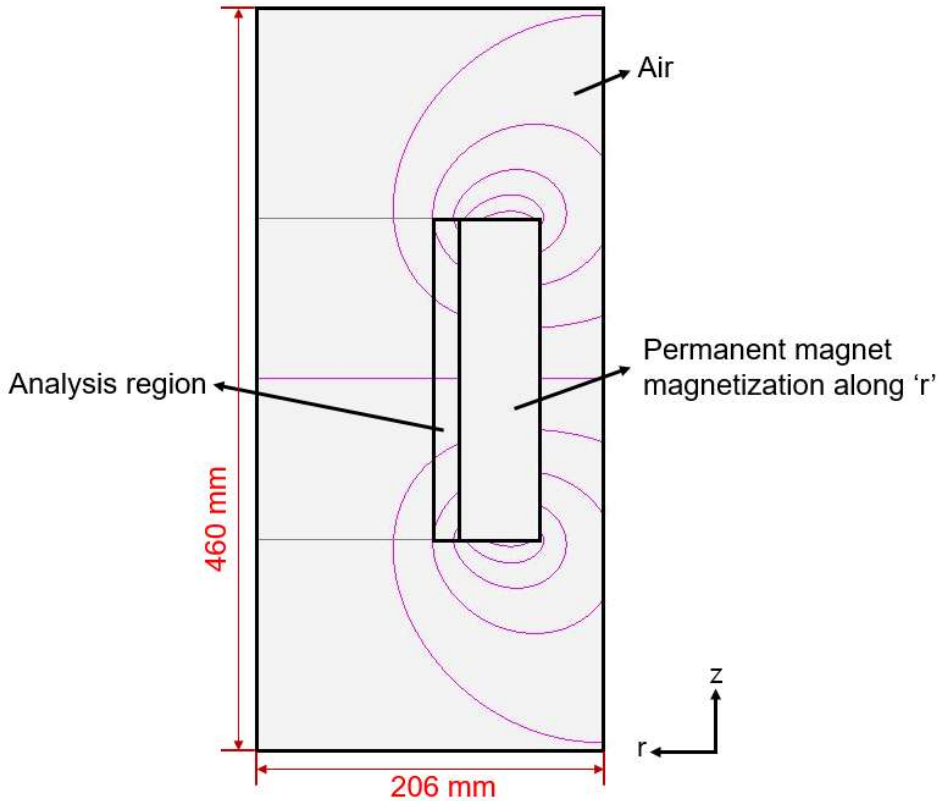
Air
Permanent magnet
magnetization along ‘r’
Analysis region
460 mm
206 mm
z
r

Fig. 5

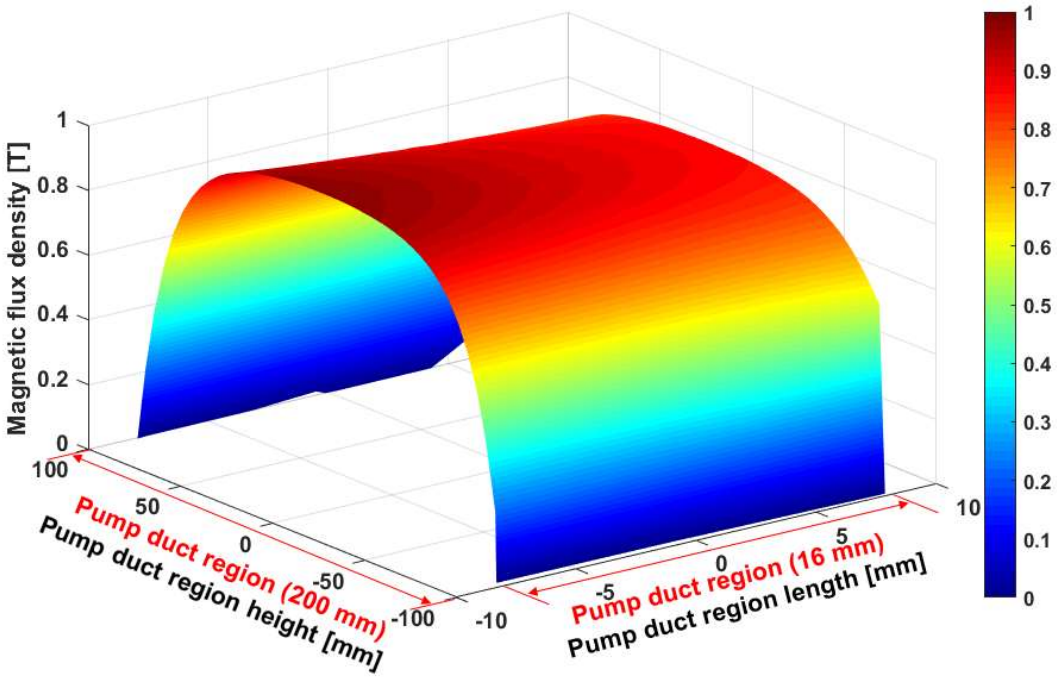
Magnetic flux density [T]
1
0.8
0.6
0.4
0.2
0
100
50
0
-50
-100
Pump duct region (200 mm)
Pump duct region height [mm]
-10
-5
0
5
10
Pump duct region (16 mm)
Pump duct region length [mm]
1
0.9
0.8
0.7
0.6
0.5
0.4
0.3
0.2
0.1
0

Fig. 6

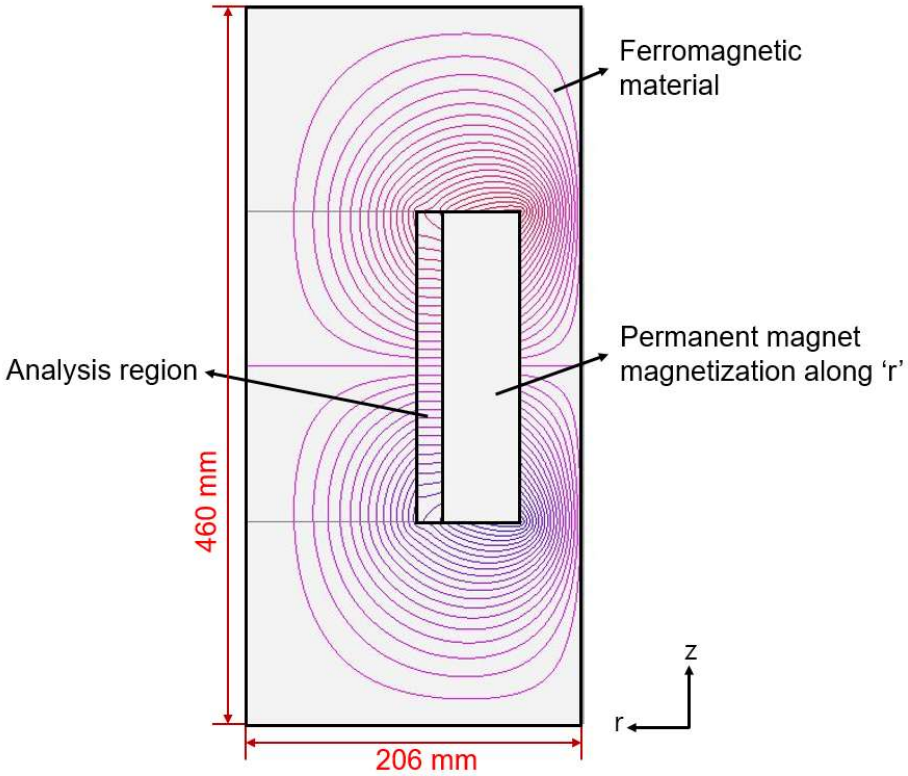
Ferromagnetic material
Permanent magnet magnetization along ‘r’
Analysis region
460 mm
206 mm
z
r

Fig. 7

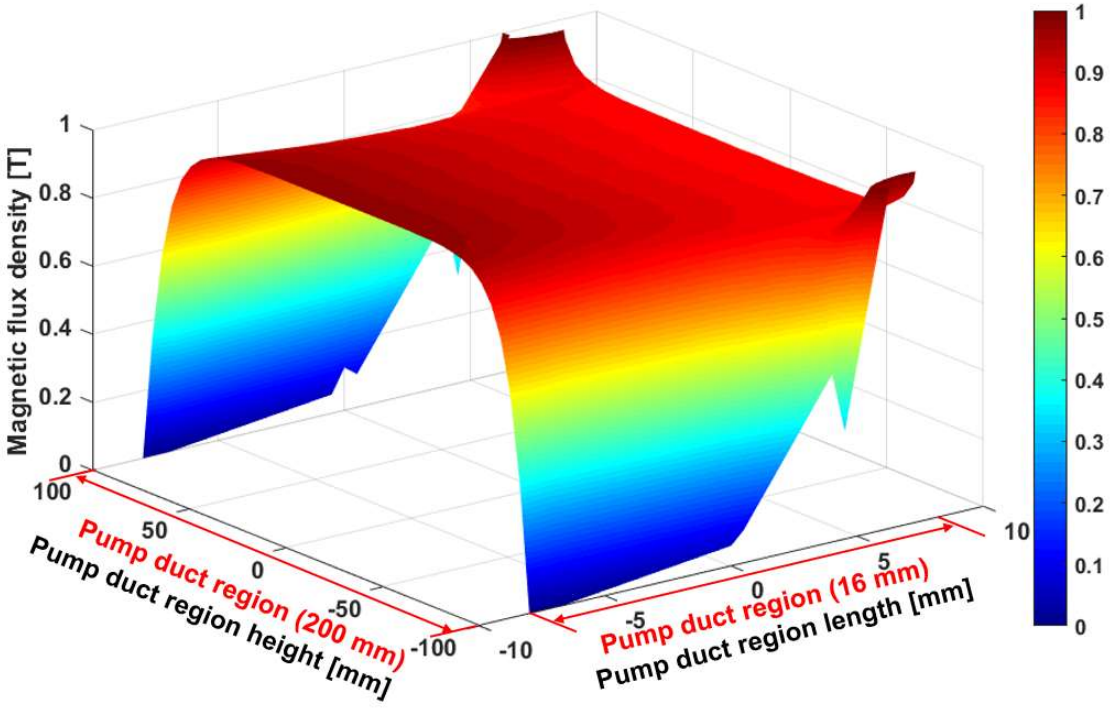
Magnetic flux density [T]
1
0.8
0.6
0.4
0.2
0
100
50
0
-50
-100
Pump duct region (200 mm)
Pump duct region height [mm]
-10
-5
0
5
10
Pump duct region (16 mm)
Pump duct region length [mm]
1
0.9
0.8
0.7
0.6
0.5
0.4
0.3
0.2
0.1
0

Fig. 8

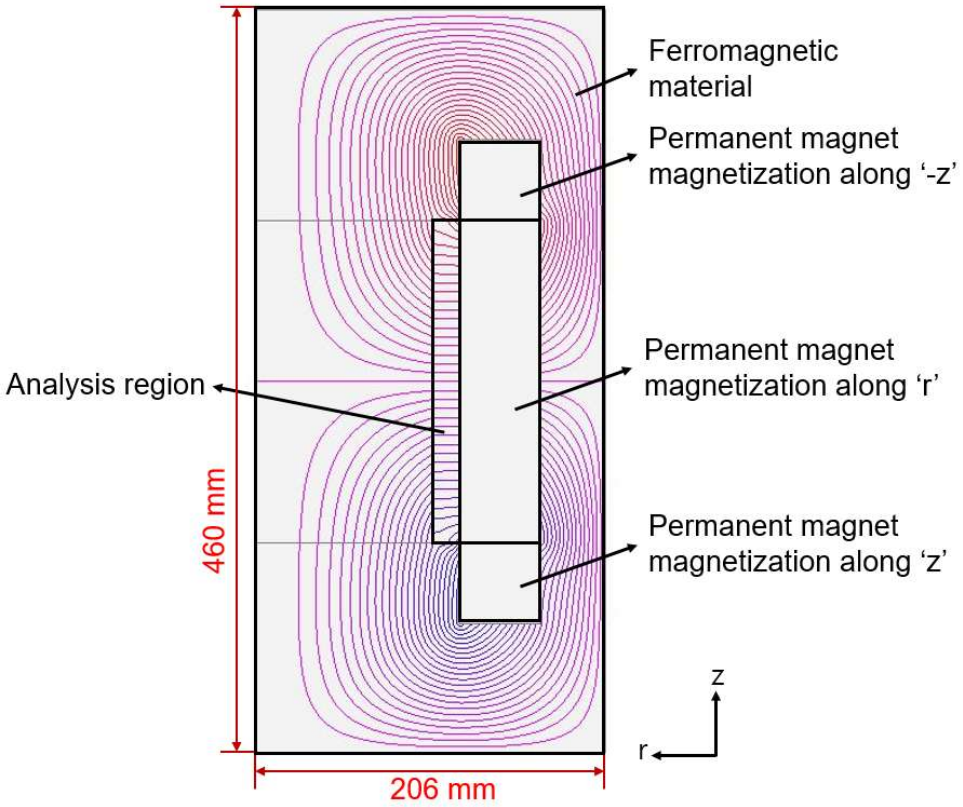
Ferromagnetic material
Permanent magnet magnetization along '-z'
Permanent magnet magnetization along 'r'
Permanent magnet magnetization along 'z'
Analysis region
460 mm
206 mm
z
r

Fig. 9

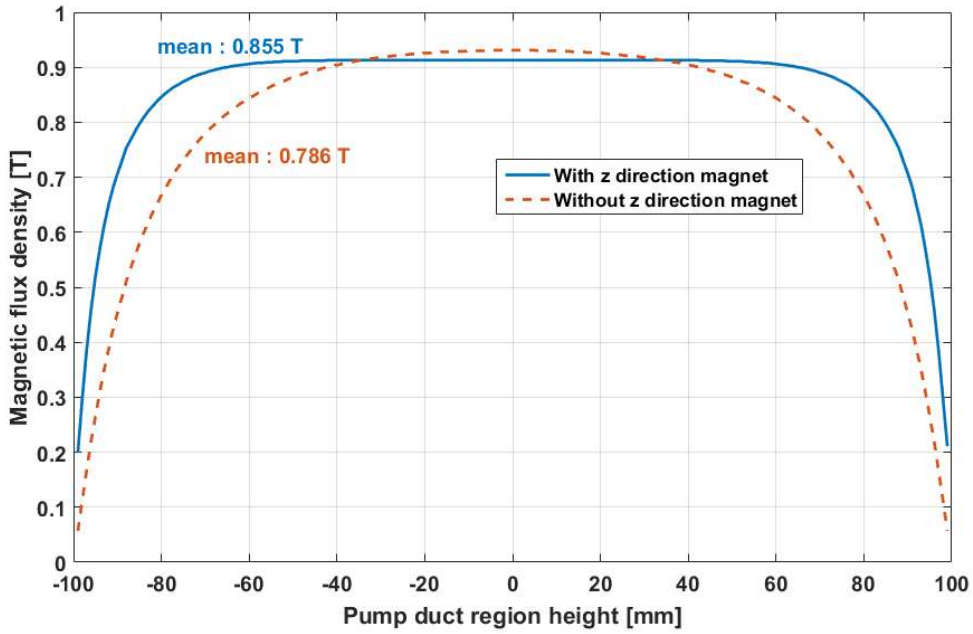
mean : 0.855 T
mean : 0.786 T
With z direction magnet
Without z direction magnet
Magnetic flux density [T]
Pump duct region height [mm]

Fig. 10

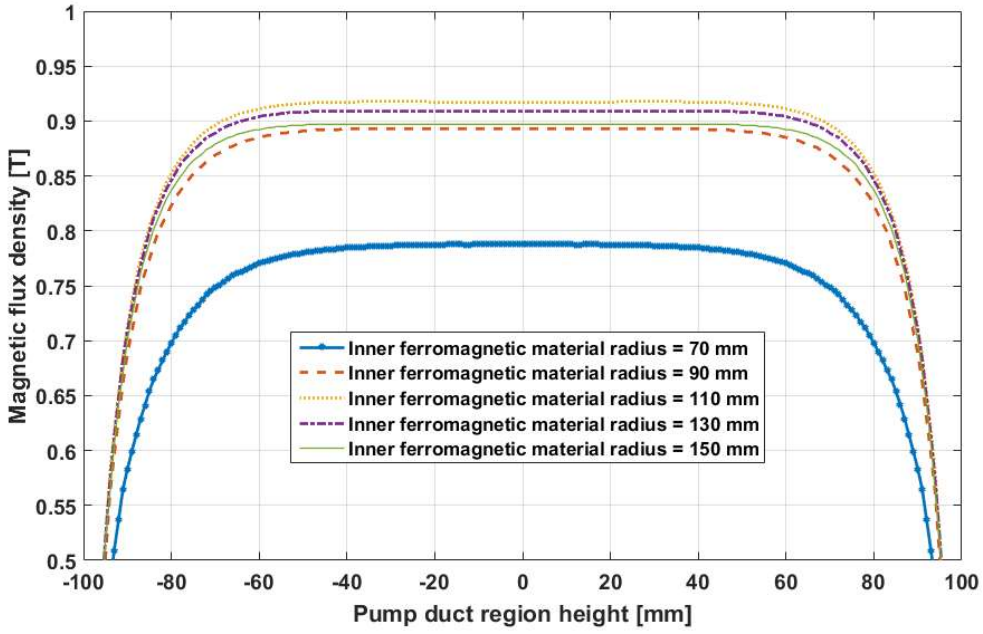
Inner ferromagnetic material radius = 70 mm
Inner ferromagnetic material radius = 90 mm
Inner ferromagnetic material radius = 110 mm
Inner ferromagnetic material radius = 130 mm
Inner ferromagnetic material radius = 150 mm
Magnetic flux density [T]
Pump duct region height [mm]

Fig. 11

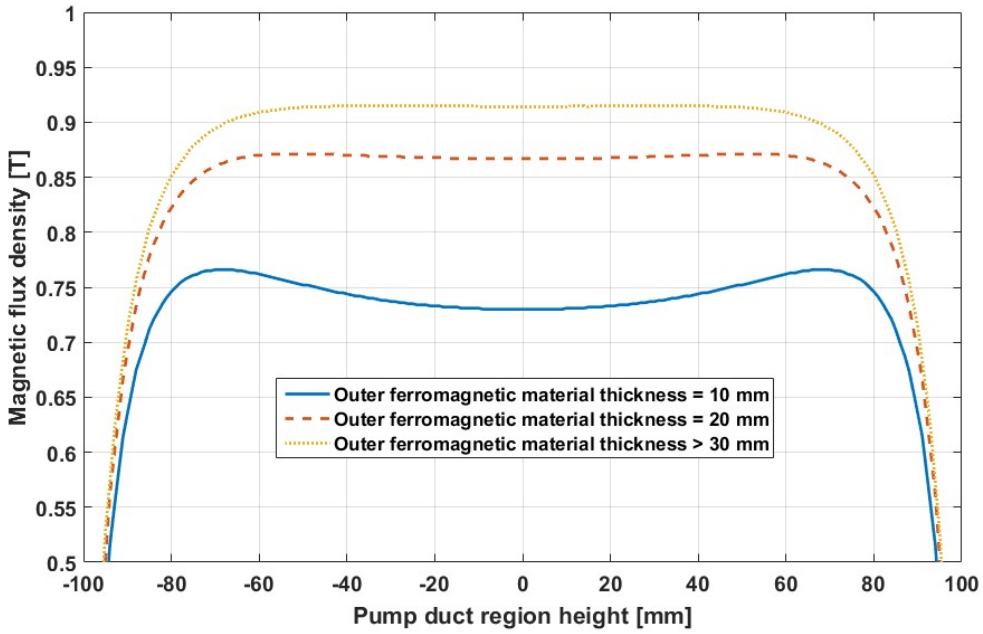
Magnetic flux density [T]
Pump duct region height [mm]
Outer ferromagnetic material thickness = 10 mm
Outer ferromagnetic material thickness = 20 mm
Outer ferromagnetic material thickness > 30 mm

Fig. 12

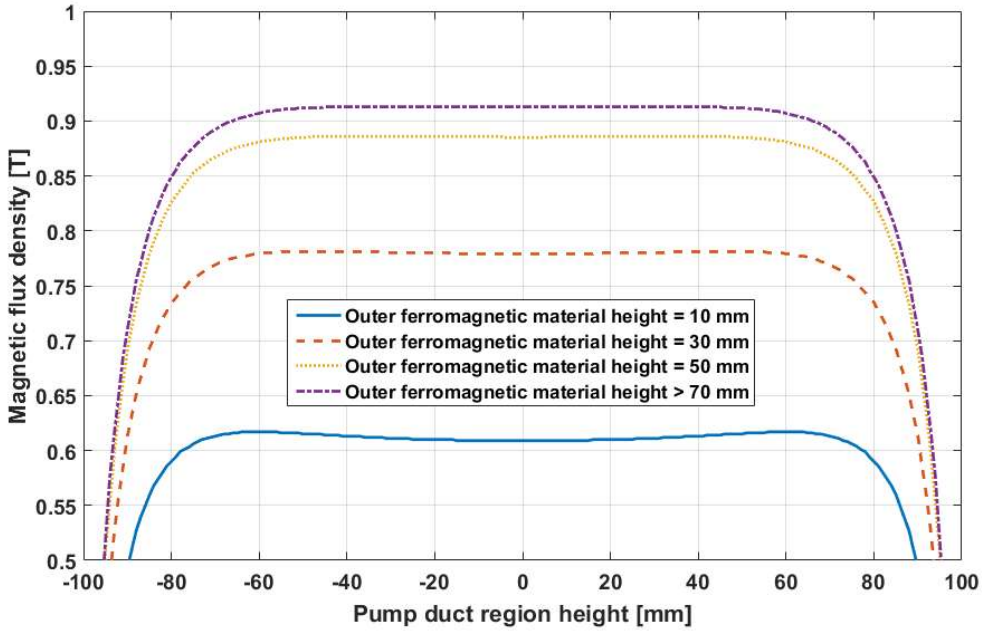
Magnetic flux density [T]
Pump duct region height [mm]
Outer ferromagnetic material height = 10 mm
Outer ferromagnetic material height = 30 mm
Outer ferromagnetic material height = 50 mm
Outer ferromagnetic material height > 70 mm

Fig. 13